Ensuring the overall combustion of herbicide metribuzin by electrochemical advanced oxidation processes. Study of operation variables, kinetics and degradation routes

Diego R. V. Guelfi [a,b], Zhihong Ye [b], Fábio Gozzi [a], Silvio César de Oliveira [a,**], Amílcar Machulek Junior [a], Enric Brillas [b], Ignasi Sirés [b,*]

[a] *Instituto de Química (INQUI), Universidade Federal de Mato Grosso do Sul, Av. Senador Filinto Muller, 1555, Caixa postal 549, MS 79070-900 Campo Grande, Brazil*

[b] *Laboratori d'Electroquímica dels Materials i del Medi Ambient, Departament de Química Física, Facultat de Química, Universitat de Barcelona, c/ Martí i Franquès 1-11, 08028 Barcelona, Spain*

Corresponding author:

*E-mail address: i.sires@ub.edu (I. Sirés)

**E-mail address: scolive@gmail.com (S.C. de Oliveira)

Abstract

This article reports the electrochemical degradation of the herbicide metribuzin (MTZ) in sulfate medium by advanced oxidation processes like anodic oxidation with electrogenerated H_2O_2 (AO-H_2O_2), electro-Fenton (EF) and UVA photoelectro-Fenton (PEF). A boron-doped diamond (BDD) anode was combined with an air-diffusion cathode with ability to produce H_2O_2. Unprecedented overall combustion was feasible by all methods at a constant current density (j) ≥ 100.0 mA cm^{-2}. The total organic carbon (TOC) removal achieved by AO-H_2O_2 was independent from pH within the range 3.0-9.0, whereas the oscillatory dependence of the pseudo-first-order MTZ decay rate constant with this variable was ascribed to adsorption on the BDD surface. In EF and PEF at pH 3.0, 0.50 mM Fe^{2+} was determined as optimum catalyst content and the MTZ removal showed two consecutive pseudo-first-order kinetic stages. These were related to the fast reaction of the target molecule with $^{\bullet}OH$ formed from Fenton's reaction, followed by a slower attack of physisorbed BDD($^{\bullet}OH$) onto Fe(III)-MTZ complexes. The effect of j and MTZ content on decay kinetics and TOC removal was examined. PEF was the best treatment due to the decomposition of photoactive intermediates by UVA radiation, yielding total mineralization of a 0.523 mM herbicide solution after 420 min of electrolysis at 100.0 mA cm^{-2}. A thorough reaction pathway for MTZ degradation is proposed from the sixteen heteroaromatic by-products and three aliphatic molecules identified by GC-MS and LC-MS/MS. Oxalic and oxamic acids were detected as final carboxylic acids by ion-exclusion HPLC.

Keywords: Anodic oxidation; Electro-Fenton; Metribuzin; Photoelectro-Fenton; Oxidation products; Water treatment

1. Introduction

In recent times, a wide range of advanced oxidation processes (AOPs) has shown great performance for removing biorefractory organic pollutants from water [1-3]. AOPs encompass chemical, photoassisted and electrochemical methods that enable the oxidation of those xenobiotics by reaction with hydroxyl radical ($^{\bullet}$OH) generated on demand. This radical is a very strong oxidant (E^{o} = 2.80 V/SHE) that can non-selectively destroy most of the organic pollutants of concern, transforming them into CO_2 and inorganic ions. In particular, much effort is put on electrochemical AOPs (EAOPs) due to their simple setups and handling, mild operation conditions and high efficiency, yielding units at competitive rates [4-7].

From a conceptual and technological standpoint, anodic oxidation (AO) or electro-oxidation is the simplest EAOP. This method consists in the generation of physisorbed hydroxyl radical M($^{\bullet}$OH) at the anode M from electrochemical water oxidation at high current, being necessary a good transport of organics to the electrode [4,5]. It has been established that the non-active boron-doped diamond (BDD) thin-films are the best anodes for AO, owing to the large production of reactive BDD($^{\bullet}$OH) along with the weak BDD-$^{\bullet}$OH interaction, thus minimizing the transformation of the radical into less oxidizing metal oxides [4,8-11]. Progress on AO has been made by promoting the simultaneous generation of H_2O_2 at the cathode from the 2-electron reduction of injected O_2 gas via reaction (1), giving rise to the so-called AO-H_2O_2 process [6,7,11-13].

$$O_{2(g)} + 2H^+ + 2e^- \rightarrow H_2O_2 \quad (1)$$

Carbonaceous cathodes [14,15], including carbon felt [16,17] and hydrophobized porous carbon-polytetrafluoroethylene (PTFE) gas-diffusion materials [11,18,19], ensure the high efficiency of reaction (1). The latter group is particularly interesting due to the excellent resistance in all aqueous media, along with a high catalytic ability to produce H_2O_2 [20-22].

The H_2O_2 generated in AO-H_2O_2 is not very powerful as compared to M($^{\bullet}$OH). However, it can be activated using Fenton-based EAOPs under acidic conditions, thereby enhancing the decontamination. In electro-Fenton (EF), Fe^{2+} is added as catalyst since it reacts with H_2O_2 originating Fe^{3+} ion and homogeneous $^{\bullet}$OH via the well-known Fenton's reaction [5,16,17]. As a result, both hydroxyl radicals (M($^{\bullet}$OH) and $^{\bullet}$OH) attack the organic molecules. The resulting Fe^{3+} ion can be reduced at the cathode to produce again the Fe^{2+} ion. One limitation of this method is the production of complexes of Fe(III) with intermediates like carboxylic acids, which present a slow decay kinetics upon reaction with hydroxyl radicals [5,7]. Photoelectro-Fenton (PEF) overcomes this problem because the solution is illuminated with UVA light to photolyze these complexes [5,18,19,21]. Moreover, additional quantities of homogeneous $^{\bullet}$OH are produced from Fe(III) photoreduction.

The effectiveness of the above Fenton-based EAOPs for wastewater treatment has been well proven for many organic pollutants. The use of BDD anode is sometimes advantageous, especially in the case of AO and AO-H_2O_2 [5-7,12-15]. In earlier work, we described the total mineralization of a symmetrical triazine like atrazine, a common herbicide, in acidic sulfate medium by means of AO, AO-H_2O_2, EF and PEF with a BDD anode [23,24]. This was a significant achievement in practice since atrazine is only converted to cyanuric acid upon application of other AOPs, thereby demonstrating the prevailing oxidative role of BDD($^{\bullet}$OH). In contrast, much less is known about the electrochemical removal of asymmetrical triazine herbicides, being necessary to ascertain the performance of these electrochemical methods.

Metribuzin (MTZ, 4-amino-6-*tert*-butyl-3-(methylsulfanyl)-1,2,4-triazin-5(4*H*)-one, $C_8H_{14}N_4OS$, M = 214.29 g mol^{-1}) is an asymmetrical triazine or triazinone pre- and post-emergence herbicide widely used in crops including sugar cane, tomatoes, potatoes and soy bean. It inhibits the photosynthesis by disrupting photosystem II. MTZ has been detected in surface water of Spain [25], Greece [26], USA [27], Brazil [28] and Australia [29] at

concentrations lower than 0.5 μg L^{-1}. Its toxicity over fishes has been documented, promoting loses of weight and total body length with inhibition of specific growth rate [30]. Several authors have described the decay of MTZ concentration and, in some cases, the detection of heteroaromatic by-products resulting from: (i) adsorption with granular activated carbon [31] and fungal biomass [32], (ii) ozonation [33], (iii) chlorination [34], (iv) photolysis with UVC light [35], (v) electrocoagulation with Fe anode under UVC radiation [36] and (vi) heterogeneous photocatalysis with ZnO under sunlight [37] and with TiO_2 under UVA light [38] or simulated sunlight [39]. The latter work also reported that only 80% of total organic carbon (TOC) was reduced after 300 min of photocatalytic treatment of a suspension with 10 mg L^{-1} MTZ and 100 mg TiO_2, with irradiance of 750 W m^{-2}.

The aim of this study is to assess the removal of MTZ by AO-H_2O_2, EF and PEF with a BDD anode in order to establish if it can be completely mineralized. The effect of different operation variables such as solution pH, applied current density (*j*), and Fe^{2+} and herbicide concentrations, as well as the alternative use of Fe^{3+} as catalyst, was examined. The MTZ decay was followed by high-performance liquid chromatography (HPLC), whereas the mineralization was monitored from TOC removal. The main degradation routes are proposed from the intermediates detected by gas chromatography-mass spectrometry (GC-MS), liquid chromatography-MS (LC-MS/MS) and ion-exclusion HPLC.

2. Materials and methods

2.1. Reagents

Metribuzin (> 98% purity) was of analytical grade purchased from Sigma-Aldrich. Oxalic and oxamic acids were of analytical grade supplied by Panreac. H_2SO_4, NaOH, Na_2SO_4, $FeSO_4 \cdot 7H_2O$ and $Fe(NO_3)_3 \cdot 9H_2O$ were of analytical grade purchased from Vetec Quimica

Fina and Merck. Solutions were prepared with ultrapure water (Millipore Milli-Q, resistivity > 18.2 MΩ cm).

2.2. Electrochemical systems

All the assays were performed with 100 mL of herbicide solutions, which contained 0.050 M Na_2SO_4 as supporting electrolyte. The initial pH was adjusted with 0.1 M H_2SO_4 or 0.1 M NaOH. The electrolytic trials were carried out in a thermostated, open, one-compartment glass tank reactor, which was kept at 25 ºC. The solution was magnetically stirred at 700 rpm with a PTFE follower. The anode was a 3 cm^2 BDD electrode supplied by NeoCoat (La Chaux-de Fonds, Switzerland) as a thin-film deposited on single-crystal *p*-type Si (100) wafers (0.1 Ω cm, Siltronix). The cathode was a 3 cm^2 carbon-PTFE air-diffusion electrode supplied by E-TEK (Somerset, NJ, USA). It was mounted as reported elsewhere [18] and fed with compressed air for continuous H_2O_2 generation. The separation between the electrodes was near 1 cm. The trials were made galvanostatically and the constant current was provided by an Agilent N5765A DC or an Instrutherm Fa-3003 power supply. The EF and PEF treatments were ran after addition of Fe^{2+} as catalyst, usually 0.50 mM. A Philips TL/4W/08 fluorescent black light tube lamp (λ_{max} = 360 nm), placed at about 5 cm over the solution surface, was used as illumination source in PEF. The influence of Fe^{3+} as catalyst was examined as well.

2.3. Instruments and analytical procedures

A Crison 2000 pH-meter was utilized to determine the solution pH. Samples were filtered with Whatman 0.22 μm PTFE filters before analysis. In order to determine the MTZ concentration in EF and PEF, the samples were diluted with acetonitrile (1:1, *v*/*v*) upon withdrawal, thus preventing further degradation. The herbicide content was determined by reversed-phase HPLC. The system consisted in a Thermo Scientific Finnigan Surveyor liquid chromatograph, fitted with an Agilent Technologies Zorbax Eclipse XDB-C-18 5 μm, 250

mm × 4.6 mm, column, which was coupled to a photodiode array detector selected at λ = 298 nm. A 50:50 (*v*/*v*) methanol/water mixture was eluted at 0.7 mL min^{-1} as mobile phase. The peak associated with MTZ appeared at 11.9 min, showing a limit of detection (LOD) = 1.08×10^{-2} mg L^{-1} and a limit of quantification (LOQ) = 3.6×10^{-2} mg L^{-1}.

The generated carboxylic acids were quantified by ion-exclusion HPLC following the procedure reported in earlier work [18]. The NH_4^+ concentration of samples was obtained from standard method SM 4500NH3 B/C [40], whereas NO_3^- and SO_4^{2-} were quantified using the EPA method 300.0 (Revision 2.1., 1993) [41].

TOC was measured on a Shimadzu TOC-V CPN analyzer. Reproducible values with 1% accuracy were obtained by injecting 50 μL of samples previously diluted (1:3, *v/v*) with Milli-Q water (LOD = 0.180 mg L^{-1}, LOQ = 0.530 mg L^{-1}).

Released inorganic ions were quantified after 540 min of EF treatment of a 0.523 mM MTZ solution with 0.50 mM Fe^{2+}, at pH 3.0 and j = 100.0 mA cm^{-2}, which yielded a TOC abatement of 99% (see below). It was found that the initial S of the herbicide (0.523 mM) was completely transformed into SO_4^{2-} ion (0.520 mM). In contrast, most of initial N (2.092 mM) did not remain in the solution, probably due to transformation into N_2 or volatile N_xO_y [7,42]. Only a small proportion was detected as NH_4^+ (0.39 mM, 18.6% of initial N) and NO_3^- (0.42 mM, 20.1% of initial N) ions. Based on these findings, the total mineralization for MTZ can be expressed as follows:

$$C_8H_{14}N_4OS + 25H_2O \rightarrow 8CO_2 + 2NO_3^- + 2NH_4^+ + SO_4^{2-} + 56H^+ + 54e^- \quad (2)$$

Considering that this reaction was verified for all the EAOPs tested, the mineralization current efficiency (MCE, in %) at given time t (in h) of a given assay at current I (in A) was calculated from Eq. (3) [42]:

$$\%\ \mathrm{MCE} = \frac{nFV\Delta\mathrm{TOC}}{4.32\mathrm{x}10^7 mIt}100 \quad (3)$$

where n is the number of electrons consumed for the overall combustion (= 54, from reaction (2)), F is the Faraday constant, V is the solution volume (in L), ΔTOC is the abated TOC (in mg L^{-1}) at time t, 4.32×10^7 is a conversion factor (3,600 s h^{-1} × 12,000 mg C mol^{-1}) and m is the number of carbon atoms of MTZ.

Duplicate experiments were carried out, and the average values obtained are reported. The bar errors with 95% confidence interval are shown in the figures.

The oxidation by-products with enough stability to become accumulated for a certain amount of time were collected at 15 and 120 min of AO-H_2O_2 and 5 and 45 min of EF treatments of 0.523 MTZ solutions made at pH 3.0 and j = 100.0 mA cm^{-2}. Then, they were detected and identified by GC-MS and LC-MS/MS. For each treated solution, the extraction of organics was made with CH_2Cl_2 (25 mL × 3). After mixing up, each resulting organic solution was dried over Na_2SO_4, filtered and evaporated under reduced pressure to obtain less than 1 mL. For the GC-MS analysis, the procedure described in earlier work was followed [19], and NIST05-MS library was utilized to interpret the mass spectra obtained. The LC-MS/MS analysis was performed with a Shimadzu LC-20AD pump, fitted with a Kinetex C-18 2.6 μm, 150 mm × 2.2 mm, column at 50 ºC, and coupled to a Bruker Daltonics Microtof-QIII mass spectrometer, with electrospray ionization source (EIS) and triple-quadrupole mass spectrometer and time-of-flight in positive ionization mode. The mobile phase was composed of a linear gradient of water (A) and acetonitrile (B), both with 1% acetic acid, eluted at 0.3 mL min^{-1} as follows: 3% B for 2 min, 3% to 25 % B from 2 to 25 min, 25% to 80% B from 25 to 40 min and constant for 3 min, 80% to 3% B from 43 to 44 min, and 3% B up to 48 min.

3. Results and discussion

3.1. AO-H_2O_2 treatment of MTZ solutions

The performance of the AO-H_2O_2 process was assessed for 100 mL of 0.523 mM herbicide (112.0 mg L^{-1}, 50 mg L^{-1} of TOC) solutions in 0.050 M Na_2SO_4 using a stirred BDD/air-diffusion tank reactor at 25 ºC. The effect of the solution pH was investigated by adjusting it to 3.0, 5.0 or 9.0, carrying out the electrolyses at a constant j = 100.0 mA cm^{-2} for 540 min. At this high j-value, great amounts of physisorbed BDD(•OH) are expected from reaction (4) [4,8-11], which is a much stronger oxidant as compared to H_2O_2 continuously generated at the cathode from reaction (1). Along these assays, the solutions became more acid due to the formation of carboxylic products [5-7].

$$BDD + H_2O \rightarrow BDD(^{\bullet}OH) + H^+ + e^- \quad (4)$$

Fig. 1a highlights a rapid exponential abatement of MTZ in all the assays, although its decay rate depended on pH. The herbicide disappeared in 180 min at pH 3.0 and 240 min at pH 5.0, only requiring 120 min at pH 9.0. The concentration decays agreed with a pseudo-first-order decay kinetics, as shown in the inset of Fig. 1. This behavior suggests the attack of a constant and small quantity of BDD(•OH) on MTZ, and its increase led to a quicker abatement. The apparent rate constants ($k_{app,1}$) and the good R^2-value obtained are listed in Table 1. As expected, the higher $k_{app.1}$-value was achieved at pH 9.0, whereas the lowest one was found at pH 5.0. This oscillating tendency is difficult to understand because the same structure of the neutral MTZ molecule (pK_b = 13.0 [34]) was the main electroactive species within the pH range tested. One can then hypothesize that the change in $k_{app,1}$ is related to the adsorption ability of MTZ molecules onto the BDD surface, thereby favoring the attack of BDD(•OH) as occurs at pH 9.0.

In contrast, Fig. 1b depicts a continuous and slow TOC removal for all solutions, with no significant effect of pH, reaching an almost total mineralization with 95-96% TOC abatement

at 540 min (see Table 1). It is thus evident that all the intermediates formed along the mineralization were destroyed at a similar rate. This is confirmed by the analogous profiles of MCE depicted in the inset panel of Fig. 1b, with maximal values ranging between 3.8% and 4.2% at 120 min, finally decreasing to about 2.6% (see Table 1). The drop of MCE with prolonging electrolysis time can be explained by the generation of by-products that are more hardly destroyed by BDD($^{\bullet}$OH), as well as the global loss of organic load [4].

The above findings demonstrate the good oxidation power of the BDD to destroy the herbicide and its oxidation by-products at all pH values, giving rise to almost overall mineralization. The EF process was further tested at pH 3.0, as discussed in the next section.

3.2. Treatment of acidic MTZ solutions by EF

First, the catalyst content for the removal of MTZ in acidic sulfate medium was optimized at pH 3.0, which is the optimal for Fenton's reaction (5) between added Fe^{2+} and produced H_2O_2 [5-7]. This is a key parameter to enhance the $^{\bullet}$OH generation.

$$Fe^{2+} + H_2O_2 \rightarrow Fe^{3+} + {}^{\bullet}OH + OH^- \quad (5)$$

The assays were carried out with 0.523 mM herbicide solutions by changing the Fe^{2+} concentration between 0.10 and 1.50 mM, at j = 100.0 mA cm^{-2}. The initial pH 3.0 practically did not vary during 540 min. Fig. 2a shows a slow MTZ decay at 0.10 mM Fe^{2+}, with total disappearance at 150 min. The removal was accelerated at all greater concentrations, with similar decay profiles and complete disappearance at 105 min. Furthermore, a significant removal can be observed during the first 2 min in these cases, being less evident at 0.10 mM Fe^{2+}. As a result, two consecutive linear correlations were obtained from the pseudo-first-order kinetic analysis of MTZ decays at each catalyst concentration, as presented in the inset panel of Fig. 2a. The existence of two different kinetic stages confirms our recent work on the treatment of N-containing aromatic pesticides [18,19], and can be ascribed to a change in various species and main oxidizing agent, as follows: (i) the first region corresponds to the

rapid reaction between MTZ and $^{\bullet}OH$ formed from Fenton's reaction (5), whereas (ii) the second region can be explained by the much slower action of BDD($^{\bullet}OH$) on MTZ complexes with Fe(III) originated from reaction (5). The formation of such complexes will be evidenced in the study about the PEF treatment discussed in section 3.3. Table 1 summarizes the evident rise of the apparent rate constant for the first region ($k_{app,1}$) when the Fe^{2+} concentration was increased from 0.10 to 0.50 mM, which can be accounted for by the enhanced $^{\bullet}OH$ production from Fenton's reaction (5). The subsequent progressive drop of $k_{app,1}$ upon use of 1.00 and 1.50 mM Fe^{2+} can be associated with a higher destruction of the excess of $^{\bullet}OH$ by parasitic reaction (6), favoring the Fe^{3+} accumulation. Once the Fe(III)-MTZ species became predominant over uncomplexed MTZ, which usually occurred after 6-7 min of electrolysis (see Fig. 2a), its oxidation by BDD($^{\bullet}OH$) was the main degradation route. Note that the apparent rate constant for the second region ($k_{app,2}$) was about 35-44% smaller at 0.10 mM Fe^{2+}, as compared to the other catalyst contents (see Table 1). Such lower $k_{app,2}$-value may be related to the smaller quantity of Fe(III)-MTZ complexes produced, whereas the quite similar $k_{app,2}$-values at 0.50-1.50 mM Fe^{2+} agrees with the analogous MTZ decay profiles of Fig.2a, being independent of the amount of $^{\bullet}OH$ produced in the bulk.

$$Fe^{2+} + {}^{\bullet}OH \rightarrow Fe^{3+} + OH^{-} \quad (6)$$

A continuous TOC decay can be observed in Fig. 2b for the above experiments. The TOC of the solution with 0.10 mM Fe^{2+} was reduced by 91%, being upgraded to 98-99% at 0.50 and 1.00 mM Fe^{2+}. In contrast, at the highest Fe^{2+} content, the profile was rather analogous to that obtained at the lowest one. This tendency is the same as that explained above for $k_{app,1}$ related to the production of $^{\bullet}OH$ in the system, thus suggesting an important role of this radical, along with BDD($^{\bullet}OH$), to mineralize all the intermediates. The inset panel of Fig. 2b shows the MCE-time plots for these assays. The highest MCE was found at 0.50 mM Fe^{2+}, yielding values between 4.6% and 4.9% up to 300 min, which dropped to 2.7% at 540 min

253 (see Table 1). An analogous behavior can be observed for the other catalyst concentrations,
254 with lower maximal and final MCE values of 2.5-2.7% (see Table 1).

255 The above findings allow concluding that 0.50 mM Fe^{2+} was the optimum concentration
256 for the EF treatment of MTZ solutions and hence, it was chosen for further trials.

257 Another important experimental variable that affects the $^{\bullet}OH$ production is the *j*-value.
258 The effect of this parameter was assessed using a 0.523 mM MTZ solution in 0.050 M
259 Na_2SO_4 at 0.50 mM Fe^{2+}, pH 3.0 and 25 ºC, working between 33.3 and 100.0 mA cm^{-2}. The
260 concentration abatements for these trials are presented in Fig. 3. A fast decay, which became
261 more pronounced as *j* rose, was observed at short time (first kinetic stage), being followed by
262 a slower removal (second kinetic stage). Total disappearance was more rapidly reached as *j*
263 was increased, needing 210, 180 and 105 min upon use of 33.3, 66.7 and 100.0 mA cm^{-2},
264 respectively. The two consecutive linear trendlines obtained from the pseudo-first-order
265 analysis of concentration decays are depicted in the inset of Fig. 3a. The data of Table 1 show
266 that both, $k_{app,1}$- and $k_{app,2}$-values, became greater at increasing *j*. This is not surprising
267 because more hydroxyl radicals are expected to be produced as *j* grows [5-7,14,15,42]. This
268 occurs thanks to the acceleration of reaction (4) that yields larger quantities of BDD($^{\bullet}OH$),
269 and that of reaction (1) that allows a larger production of H_2O_2, which in turn promotes the
270 generation of greater amount of $^{\bullet}OH$ from Fenton's reaction (5).

271 The promotion of generated oxidants also explains the quicker TOC abatement at higher
272 *j*, as seen in Fig. 3b. The slower TOC decays at 33.3 and 66.7 mA cm^{-2} led to 90% and 92%
273 mineralization at 540 min, in contrast to 99% obtained at the highest *j* of 100.0 mA cm^{-2} (see
274 Table 1). This means that total combustion of MTZ can be attained by EF operating at current
275 densities ≥ 100.0 mA cm^{-2}. Conversely, the corresponding MCE values depicted in the inset
276 panel of Fig.3b present the opposite tendency, because the most efficient process was that
277 performed at 33.3 mA cm^{-2}. Under these conditions, 8.7% was the maximum MCE value

278 determined at 60 min, dropping to 7.9% at the end. Lower final MCE values were determined
279 at increasing *j* (see Table 1). This behavior is typically reported for EAOPs, being ascribed to
280 the enhancement of parasitic reactions. The most important among such undesired reactions is
281 the oxidation of BDD($^{\bullet}$OH) to O_2, largely enhanced as *j* is risen [4,5]. Other relevant parasitic
282 reactions involve the $^{\bullet}$OH dimerization to H_2O_2, and its consumption by the latter species to
283 yield the weaker oxidant hydroperoxyl radical ($HO_2^{\bullet}$) [5,17,24].

284 The last experimental variable tested was the herbicide concentration, which needs to be
285 assessed in order to elucidate the ability of EF to destroy concentrated solutions. Fig. 4a
286 shows the time course of the normalized MTZ content, employing solutions with initial
287 concentrations from 0.262 to 1.046 mM, upon treatment with 0.50 mM Fe^{2+} at pH 3.0 and *j* =
288 100.0 mA cm^{-2}. The degradation was decelerated at higher herbicide content, reaching
289 complete removal at increasing times of 90, 105 and 180 min for 0.262, 0.523 and 1.046 mM,
290 respectively. This can also be deduced from the data of Table 1, since the $k_{app,1}$- and $k_{app,2}$-
291 values (determined from the kinetic analysis of the inset of Fig. 4a) underwent a gradual drop,
292 more apparent between 0.523 and 1.046 mM. This behavior can be explained by a progressive
293 reduction of the available $^{\bullet}$OH and BDD($^{\bullet}$OH) to attack the uncomplexed molecule and its
294 Fe(III) complexes, respectively, because a large proportion of both radicals participates in the
295 competitive oxidation of oxidation by-products formed. Fig. 4b confirms this fact, since quick
296 and analogous removals of normalized TOC can be observed for all the MTZ concentrations
297 tested, attaining 97%-99% mineralization at the end (see Table 1). The destruction of more
298 carbon at a given time is indicative of a more efficient removal of intermediates. This is
299 reflected in the corresponding MCE-time plots presented in the inset of Fig. 4b, where the
300 MCE values grew with MTZ content (see Table 1). The greater efficiencies were then
301 obtained at the highest (1.046 mM) concentration, which decayed from 11.2% at 30 min to
302 5.4% at 540 min. Since all these trials were performed at *j* = 100.0 mA cm^{-2}, the same amount

of BDD(•OH) and •OH are expected to be formed. The enhanced destruction at increasing herbicide concentration can then be accounted for by the existence of greater amounts of both radicals that are available from the deceleration of their parasitic reactions, due to the preferential attack over organics.

The aforementioned findings allow inferring that the EF process with a BDD/air-diffusion cell is powerful enough to destroy all the intermediates of MTZ, even at high concentrations, using 0.50 mM Fe^{2+} as catalyst and j values $\geq$ 100 mA cm^{-2}.

3.3. PEF treatment with Fe^{2+} and Fe^{3+} as catalysts

The PEF treatment of a 0.523 mM herbicide solution was made under the best conditions found for EF (0.50 mM Fe^{2+}, j = 100.0 mA cm^{-2}) under irradiation with a 4 W UVA lamp. Fig. 5a and b present the corresponding concentration and TOC decays for this trial. The concentration abatement in PEF was quite similar to that obtained by EF, yielding total removal at 105 min in both cases (see Fig. 2a). From the kinetic analysis, as depicted in the inset panel of Fig. 5a, similar $k_{app,1}$- and $k_{app.2}$-values were found for both processes (see Table 1). This means that the uncomplexed molecule and its Fe(III) complexes were removed by a similar amount of oxidizing agents in both cases, without significant influence of incident light. In contrast, Fig. 5b highlights that complete combustion of MTZ was achieved at 420 min of PEF, a time much shorter than 540 min required in EF (see Fig. 2b). The greater mineralization power of PEF can be related to the photolysis of some intermediates by UVA light, which accelerates their destruction by BDD(•OH) and/or •OH.

It has been established that when a gas-diffusion cathode is used in Fenton-based EAOPs, most of the Fe^{2+} added as catalyst is converted into Fe^{3+}, due to the low ability of this material to reduce the ferric ion [5]. This could explain the fast change from free MTZ to Fe(III)-MTZ complexes, responsible for the appearance of two distinct kinetic regions. To corroborate the formation of such complexes, an additional PEF trial was performed, but directly using 0.50

328 mM Fe^{3+} as catalyst in order to operate with a low concentration of $^{\bullet}OH$ formed from
329 Fenton's reaction (5). Under these conditions, MTZ underwent a continuous abatement,
330 disappearing at 60 min, a time shorter than that needed in PEF with Fe^{2+} (see Fig. 5a). The
331 corresponding $k_{app,1}$ = 0.0611 min^{-1}, determined from the excellent linear correlation presented
332 in the inset of Fig. 5a, was 3.2-fold higher than that found in AO-H_2O_2 under comparable
333 conditions (see Table 1). This means that the Fe(III)-MTZ complexes are more rapidly
334 destroyed than the free molecule under the action of BDD($^{\bullet}OH$). The same behavior can be
335 inferred considering the $k_{app,2}$-values for EF and PEF with Fe^{2+}, although they were only 1.7-
336 1.9 fold higher than $k_{app,1}$ for AO-H_2O_2. On the other hand, the greater $k_{app,1}$-value found in
337 PEF with Fe^{3+} as compared to the $k_{app,2}$-value for PEF with Fe^{2+} can be explained by the
338 greater amount of Fe(III)-MTZ complexes formed in the former case, being more rapidly
339 destroyed by BDD($^{\bullet}OH$). Nevertheless, Fig. 5b reveals a slightly faster TOC removal in PEF
340 with Fe^{3+} up to 240 min of electrolysis, as can also be seen in the MCE values shown in the
341 inset. At longer time, TOC was more rapidly reduced using Fe^{2+}, suggesting the generation of
342 a larger quantity of photoactive products by $^{\bullet}OH$, which are more quickly photolyzed until
343 reaching their mineralization. For PEF with Fe^{3+}, an almost total mineralization with 98%
344 TOC reduction and 2.7% MCE was finally attained (see Table 1).

345 Our results show that the PEF process with Fe^{2+} using a BDD/air-diffusion cell is the
346 most powerful EAOP to completely destroy MTZ and its oxidation products. The use of Fe^{3+}
347 as catalyst favors the degradation of the herbicide, but causes a slower mineralization.

348 *3.4. Identification of by-products*

349 Several MTZ solutions treated by AO-H_2O_2 and EF at j = 100.0 mA cm^{-2} during different
350 times were analyzed by GC-MS and LC-MS/MS to detect the most stable by-products
351 formed. Table S1 in Supplementary Material summarizes the name, molecular structure and
352 m/z values of eleven intermediates of MTZ (**1**), which include ten heteroaromatic compounds

and methylthiocyanate (**18**), identified by GC-MS. The heteroaromatic intermediates arise from the nitrosation of the lateral $–NH_2$ group (**3**), demethylation (**5** and **16**), loss of the lateral $–S-CH_3$ group (**6**), carbonylation (**7** and **12**), deamination (**8**), oxidation of the lateral –C-C- bonds with demethylation (**9**) and desulfuration (**11**), and sulfonation (**10**). Table S2 summarizes the molecular structure and exact *m*/*z* value ($+1H^+$) of nine heteroaromatic compounds and two aliphatic products (**19** and **20**) detected by LC-MS/MS. Apart from compounds **6**, **7** and **8** also found by GC-MS, other heteroaromatic stuctures were formed from dihydroxylation of **1** (**2**), demethylation and carbonylation of the $–S-CH_3$ group (**4**), and deamination with hydroxylation (**13**) and with demethylation and oxidation of the lateral –C-C- bonds (**14**, **15** and **17**). Moreover, a dimer by-product formed by heteroaromatics (**21**) was detected by LC-MS/MS (see Table S3). It is noticeable that some of these by-products have been described for MTZ degradation by photochemical methods, such as compounds **7**, **8** and **12** from UVC photolysis [35] and **2**, **6**, **7**, **8** and **12** from TiO_2 photocatalysis [38,39].

Fig. 6 shows the reaction pathway proposed for MTZ degradation by the EAOPs tested, based on the nineteen monomers detected. The main oxidizing agent is BDD($^\bullet$OH) and/or $^\bullet$OH, as stated above, and the routes can be valid either for the uncomplexed molecule and its Fe(III) complexes in Fenton-based EAOPs. The initial oxidation of **1** involves: (i) dihydroxylation to yield **2**, (ii) nitrosation of the lateral $–NH_2$ group, resulting in **3**, (iii) demethylation with formation of a double –C=C- bond and carbonylation of the CH_3 group linked to the S atom to produce **4**, (iv) di-demethylation leading to **5**, (v) loss of the lateral $–S-CH_3$ group to form **6**, (vi) carbonylation of the C(6) of the triazine ring originating **7**, and (vii) deamination to give **8**. Compound **7** can also be produced from oxidation of **6**, whereas **8** can arise from denitrosation of **3**. Further destruction of **5** takes place via either oxidation of the lateral single –C-C- to double bond and demethylation of $–S-CH_3$ group to lead to **9** or hydroxylation on C(3) with de-ethylation and sulfonation of the S atom producing **10**.

Subsequent oxidation of the lateral –C=C- to triple bond and hydroxylation with desulfuration of **9** gives rise to **11**. Demethylation of **7** or carbonylation of the C(6) of **8** yields **12**. In parallel, **8** can be either hydroxylated to form **13** or its *tert*-butyl group oxidized to give **14**, which is then demethylated producing **15** or loses methylene and –S-CH_3 groups generating **16**. Oxidation of the double –C=C- to triple bond and carboxylation of the –CH_3 group linked to the S atom of **15** gives **17**. Finally, the cleavage of the triazine ring leads to the linear compounds **18**, **19** and **20**.

Short-chain aliphatic carboxylic acids, usually with no more than four carbon atoms, are produced as final by-products during the degradation of aromatic compounds with benzene and naphthalene rings by EAOPs [5-7,12-19,42]. To clarify if this kind of compounds were produced from MTZ, a 0.523 mM herbicide solution with 0.50 mM Fe^{2+} was analyzed by ion-exclusion HPLC upon EF treatment at j = 100.0 mA cm^{-2}. Only two carboxylic acids with two carbon atoms, oxalic and oxamic, were detected by this technique, further being directly mineralized [5,7]. This is not surprising, taking into account the small sequences of carbon atoms present in the triazine ring of MTZ linked to a *tert*-butyl group. Fig. 7 highlights a rapid accumulation of oxamic acid up to 11.0 mg L^{-1} at 30 min, followed by quick removal to disappear at 150 min. This product was originated at the beginning of the process, whereas oxalic acid was more scarcely accumulated and appeared later, from 180 to 420 min with a maximal of 1.5 mg L^{-1} at 270 min. These findings suggest that other by-products more recalcitrant than carboxylic acids, probably compounds like **18**-**20**, remain in the solution until the end of the electrolysis.

4. Conclusions

The overall combustion of MTZ solutions is feasible using EAOPs with a BDD/air-diffusion cell at j values ≥ 100.0 mA cm^{-2}. PEF exhibited the greatest performance, with

optimum 0.50 mM Fe^{2+}, allowing the total TOC removal in 420 min owing to the combined oxidation action of BDD($^{\bullet}$OH), $^{\bullet}$OH and UVA radiation. EF led to a slower TOC reduction because of the absence of UVA light to photolyze some photoactive intermediates. The AO-H_2O_2 treatment in the pH range 3.0-9.0 also yielded an almost total mineralization with 95-96% TOC removal at the same *j* and time, confirming the high oxidation power of BDD($^{\bullet}$OH). In this method, the MTZ decay obeyed a pseudo-first-order kinetics and its apparent rate constant showed no clear dependence on pH, which was associated with the adsorption of the molecule at the BDD surface. In contrast, the MTZ abatement in EF and PEF with Fe^{2+} showed two consecutive kinetic regions. In the first region, $^{\bullet}$OH acted as main oxidant on the uncomplexed molecule, whereas the second one did not depend on the amount of this radical and was ascribed to the slow reaction of Fe(III)-MTZ complexes with BDD($^{\bullet}$OH). Both apparent rate constants in EF and PEF with Fe^{2+} rose with increasing *j* and decreasing MTZ content. GC-MS, LC-MS/MS and ion exclusion HPLC analysis of treated solutions allowed detecting twenty-two by-products, including sixteen heteroaromatic monomers, one dimer composed of heteroaromatic structures, and five aliphatic compounds like oxalic and oxamic acids.

Acknowledgements

Financial support from project CTQ2016-78616-R (AEI/FEDER, EU), as well as from FUNDECT, CAPES and CNPq (Brazil), is acknowledged. The PhD scholarship awarded to Z.H. Ye (State Scholarship Fund, CSC, China) is also acknowledged.

References

[1] M. Antonopoulou, E. Evgenidou, D. Lambropoulou, I. Konstantinou, A review on advanced oxidation processes for the removal of taste and odor compounds from aqueous media, Water Res. 53 (2014) 215-234.

[2] M.A. Oturan, J.-J. Aaron, Advanced oxidation processes in water/wastewater treatment: principles and applications. A review, Crit. Rev. Environ. Sci. Technol. 44 (2014) 2577-2641.

[3] N.S. Mishra, R. Reddy, A. Kuila, A. Rani, P. Mukherjee, A. Nawaz, S. Pichiah, A review on advanced oxidation processes for effective water treatment. Curr. World Environ. 12 (3) (2017).

[4] M. Panizza, G. Cerisola, Direct and mediated anodic oxidation of organic pollutants, Chem. Rev. 109 (2009) 6541-6569.

[5] E. Brillas, I. Sirés, M.A. Oturan, Electro-Fenton process and related electrochemical technologies based on Fenton's reaction chemistry, Chem. Rev. 109 (2009) 6570-6631.

[6] C.A. Martínez-Huitle, M.A. Rodrigo, I. Sirés, O. Scialdone, Single and coupled electrochemical processes and reactors for the abatement of organic water pollutants: a critical review, Chem. Rev. 115 (2015) 13362-13407.

[7] F.C. Moreira, R.A.R. Boaventura, E. Brillas, V.J.P. Vilar, Electrochemical advanced oxidation processes: a review on their application to synthetic and real wastewaters, Appl. Catal. B: Environ. 202 (2017) 217-261.

[8] B. Boye, P.A. Michaud, B. Marselli, M.M. Dieng, E. Brillas, C. Comninellis, Anodic oxidation of 4-chlorophenoxyacetic acid on synthetic boron-doped diamond electrode, New Diamond Frontier Carbon Technol. 12 (2002) 63-72.

[9] B. Marselli, J. Garcia-Gomez, P.A. Michaud, M.A., Rodrigo, C. Comninellis, Electrogeneration of hydroxyl radicals on boron-doped diamond electrodes, J. Electrochem. Soc. 150 (2003) D79-D83.

[10] E. Guinea, E. Brillas, F. Centellas, P. Cañizares, M.A. Rodrigo, C. Sáez, Oxidation of enrofloxacin with conductive-diamond electrochemical oxidation, ozonation and Fenton oxidation. A comparison, Water Res. 43 (2009) 2131-2138.

[11] A. Bedolla-Guzman, I. Sirés, A. Thiam, J.M. Peralta-Hernández, S. Gutiérrez-Granados, E. Brillas, Application of anodic oxidation, electro-Fenton and UVA photoelectro-Fenton to decolorize and mineralize acidic solutions of Reactive Yellow 160 azo dye, Electrochim. Acta 206 (2016) 307-316.

[12] G. Coria, I. Sirés, E. Brillas, J.L. Nava, Influence of the anode material on the degradation of naproxen by Fenton-based electrochemical processes, Chem. Eng. J. 304 (2016) 817-825.

[13] J.R. Steter, E. Brillas, I. Sirés, On the selection of the anode material for the electrochemical removal of methylparaben from different aqueous media, Electrochim. Acta 222 (2016) 1464-1474.

[14] S. Vasudevan, M.A. Oturan, Electrochemistry: as cause and cure in water pollution-an overview, Environ, Chem. Lett. 12 (2014) 97-108.

[15] P.V. Nidheesh, M. Zhou, M.A. Oturan, An overview on the removal of synthetic dyes from water by electrochemical advanced oxidation processes, Chemosphere 197 (2018) 210-227.

[16] O. Ganzenko, N. Oturan, I. Sirés, D. Huguenot, E.D. van Hullebusch, G. Esposito, M.A. Oturan, Fast and complete removal of the 5-fluorouracil drug from water by electro-Fenton oxidation, Environ. Chem. Lett. 16 (2018) 281-286.

469 [17] T. Pérez, G. Coria, I. Sirés, J.L. Nava, A.R. Uribe, Electrosynthesis of hydrogen
470 peroxide in a filter-press flow cell using graphite felt as air-diffusion cathode, J.
471 Electroanal. Chem. 812 (2018) 54-58.
472 [18] D.R.V. Guelfi, F. Gozzi, I. Sirés, E. Brillas, A. Machulek Jr., S.C. de Oliveira,
473 Degradation of the insecticide propoxur by electrochemical advanced oxidation
474 processes using a boron-doped diamond/air-diffusion cell, Environ. Sci. Pollut. Res. 24
475 (2017) 6083-6095.
476 [19] D.R.V. Guelfi, F. Gozzi, A. Machulek Jr, I. Sirés, E. Brillas, S.C. de Oliveira,
477 Degradation of herbicide S-metolachlor by electrochemical AOPs using a boron-doped
478 diamond anode, Catal. Today 313 (2018) 182-188.
479 [20] A. Galia, S. Lanzalaco, M.A. Sabatino, C. Dispenza, O. Scialdone, I. Sirés, Crosslinking
480 of poly(vinylpyrrolidone) activated by electrogenerated hydroxyl radicals: A first step
481 towards a simple and cheap synthetic route of nanogel vectors, Electrochem Commun
482 62 (2016) 64-68.
483 [21] T. Pérez, I. Sirés, E. Brillas, J.L. Nava, Solar photoelectro-Fenton flow plant modeling
484 for the degradation of the antibiotic erythromycin in sulfate medium, Electrochim. Acta
485 228 (2017) 45-56.
486 [22] C. Ridruejo, F. Centellas, P.L. Cabot, I. Sirés, E. Brillas, Electrochemical Fenton-based
487 treatment of tetracaine in synthetic and urban wastewater using active and non-active
488 anodes, Water Res. 128 (2018) 71-81.
489 [23] N. Borràs, R. Oliver, C. Arias, E. Brillas, Degradation of atrazine by electrochemical
490 advanced oxidation processes using a boron-doped diamond anode, J. Phys. Chem. A
491 114 (2010) 6613-6621.

[24] N. Oturan, E. Brillas, M.A. Oturan, Unprecedent total mineralization of atrazine and cyanuric acid by anodic oxidation and electro-Fenton with a boron-doped diamond anode, Environ. Chem. Lett. 10 (2012) 165-170.

[25] E. Herrero-Hernández, M.S. Rodríguez-Cruz, E. Pose-Ruan, S. Sánchez-González, M.S. Andrades, M.J. Sánchez-Martín, Seasonal distribution of herbicide and insecticide residues in the water resources of the vineyard region of La Rioja (Spain), Sci. Total Environ. 609 (2017) 161-171.

[26] E.N. Papadakis, A. Tsaboula, Z. Vryzas, A. Kotopoulou, K. Kintzikoglou, E. Papadopoulou-Mourkidou, Pesticides in the rivers and streams of two river basins in northern Greece, Sci. Total Environ. 624 (2018) 732-743.

[27] M.L.M. Tagert, J.H. Massey, D.R. Shaw, Water quality survey of Mississippi's Upper Pearl River, Sci. Total Environ. 481 (2014) 564-573.

[28] E.F. Dores, L. Carbo, M.L. Ribeiro, E.M. De-Lamonica-Freire, Pesticide levels in ground and surface waters of Primavera do Leste Region, Mato Grosso, Brazil, J. Chromatograph. Sci. 46 (2008) 585-590.

[29] G. Nachimuthu, N.V. Halpin, M.J. Bell, Effect of sugarcane cropping on herbicide losses in surface runoff, Sci. Total Environ. 557-558 (2016) 773-784.

[30] S. Štěpánová, P. Doleželová, L. Plhalová, M. Prokeš, P. Maršálek, M. Škoric, Z. Svobodová, The effect of metribuzin on early life stages of common carp (*Cyprinus carpio*), Pest. Biochem. Physiol. 103 (2012) 152-158.

[31] O. Kitous, H. Hamadou, H. Lounici, N. Drouiche, N. Mameri, Metribuzin removal with electro-activated granular carbon, Chem. Eng. Process.: Process Intensif. 55 (2012) 20-23.

[32] M. Behloul, H. Lounici, N. Abdi, N. Drouiche, N. Mameri, Adsorption study of metribuzin pesticide on fungus *Pleurotus mutilus*, Int. Biodeter. Biodegrad. 119 (2017) 684-695.

[33] M.O. Honório, E. Vaz de Liz Junior, R.F.P.M. Moreira, R.F. de Sena, H.J. José, Removal of metribuzin by ozonation: effect of initial concentration and pH, J. Environ. Prot. 4 (2013) 564-569.

[34] C.-Y. Hu, A.-P. Li, Y.-L. Lin, X. Ling, A.-P. Li, M. Cheng, Degradation kinetics and DBP formation during chlorination of metribuzin, J. Taiwan Inst. Chem. Eng. 80 (2017) 255-261.

[35] U. Raschke, G. Werner, H. Wilde, U. Stottmeister, Photolysis of metribuzin in oxygenated aqueous solutions, Chemosphere 36 (1998) 1745-1758.

[36] O. Yahiaoui, L. Aizel, H. Lounici, N. Drouiche, M.F.A. Goosen, A. Pauss, N. Mameri, Evaluating removal of metribuzin pesticide from contaminated groundwater using an electrochemical reactor combined with ultraviolet oxidation, Desalination 270 (2011) 84-89.

[37] J. Fenoll, P. Flores, P. Hellín, C.M. Martínez, S. Navarro, Photodegradation of eight miscellaneous pesticides in drinking water after treatment with semiconductor materials under sunlight at pilot plant scale, Chem. Eng. J. 204-206 (2012) 54-64.

[38] N. Vela, J. Fenoll, I. Garrido, S. Navarro, M. Gambín, S. Navarro, Photocatalytic mitigation of triazinone herbicide residues using titanium dioxide in slurry photoreactor, Catal. Today 252 (2015) 70-77.

[39] M. Antonopolou, I. Kontantinou, Photocatalytic treatment of metribuzin herbicide over TiO_2 aqueous suspensions: Removal efficiency, identification of transformation products, reaction pathways and ecotoxicity evaluation, J. Photochem. Photobiol. A: Chem. 294 (2014) 110-120.

[40] American Public Health Association, American Works Association, Water Environment Federation, Standard Methods for the Examination of Water and Wastewater, 22nd Ed. Washington, DC, 2012.

[41] EPA - Environmental Protection Agency - SW 846, Testing Methods for Evaluating Solid Wastes: Physical/Chemical Methods, 3rd Ed. (final update V), 2015.

[42] E.J. Ruiz, A. Hernández-Ramírez, J.M. Peralta-Hernández, C. Arias, E. Brillas, Application of solar photoelectro-Fenton technology to azo dyes mineralization: Effect of current density, Fe^{2+} and dye concentration, Chem. Eng. J. 171 (2011) 385-392.

Table 1

Pseudo-first-order rate constants, with the corresponding *R*-squared, and percentages of TOC removal and mineralization current efficiency after 540 min of treatment of 100 mL of herbicide solutions in 0.050 M Na_2SO_4 by several EAOPs with a BDD/air-diffusion cell under selected conditions at 25 ºC.

$[MTZ]_0$ (mM)	pH	$[Fe^{2+}]$ (mM)	j (mA cm^{-2})	$k_{app,1}$ (min^{-1})	R_1^2	$k_{app,2}$ (min^{-1})	R_2^2	% TOC removal	% MCE
AO-H_2O_2									
0.523	3.0	-	100.0	0.0189	0.990	-	-	95	2.6
0.523	5.0	-	100.0	0.0160	0.998	-	-	95	2.6
0.523	9.0	-	100.0	0.0231	0.982	-	-	96	2.6
EF									
0.262	3.0	0.50	100.0	0.4336	0.998	0.0389	0.985	99	1.3
0.523	3.0	0.10	100.0	0.0336	0.990	0.0211	0.983	91	2.5
0.523	3.0	0.50	33.3	0.0591	0.985	0.0079	0.984	90	7.9
0.523	3.0	0.50	66.7	0.1390	0.961	0.0167	0.989	92	3.8
0.523	3.0	0.50	100.0	0.408	0.968	0.0378	0.994	99	2.7
0.523	3.0	1.00	100.0	0.3994	0.968	0.0326	0.996	98	2.7
0.523	3.0	1.50	100.0	0.3304	0.996	0.0348	0.996	90	2.5
1.046	3.0	0.50	100.0	0.0818	0.989	0.0155	0.989	97	5.4
PEF									
0.523	3.0	0.50	100.0	0.3590	0.980	0.0348	0.977	100 [b]	3.5 [b]
0.523	3.0	0.50 [a]	100.0	0.0611	0.983	-	-	98	2.7

[a] Fe^{3+} as catalyst

[b] Data at 420 min

Figure captions

Fig. 1. Decay of: (a) metribuzin (MTZ) concentration and (b) TOC with electrolysis time for the AO-H_2O_2 treatment of 100 mL of 0.523 mM (112.0 mg L^{-1}) herbicide with 0.050 M Na_2SO_4 at pH: (○) 3.0, (□) 5.0 and (△) 9.0. A BDD/air-diffusion cell (each electrode with 3 cm^2 area) was used, at current density (*j*) of 100.0 mA cm^{-2} and 25 ºC. The inset panel of (a) depicts the pseudo-first-order kinetic analysis, and that of (b) shows the corresponding mineralization current efficiency (MCE).

Fig. 2. Influence of catalyst concentration on the variation of (a) herbicide concentration and its kinetic analysis and (b) TOC and MCE with electrolysis time for the EF treatment of 100 mL of 0.523 mM MTZ with 0.050 M Na_2SO_4 at pH 3.0 and 25 ºC, using a BDD/air-diffusion cell at j = 100.0 mA cm^{-2}. $[Fe^{2+}]_0$ = (●) 0.10 mM, (▲) 0.50 mM, (▽) 1.00 mM and (◇) 1.50 mM.

Fig. 3. Effect of *j* on the change of (a) MTZ content and its pseudo-first-order kinetic analysis and (b) TOC and MCE with electrolysis time for the EF treatment of 100 mL of 0.523 mM herbicide with 0.050 M Na_2SO_4 and 0.50 mM Fe^{2+} at pH 3.0 and 25 ºC, using a BDD/air-diffusion cell. Input *j*: (●) 33.3 mA cm^{-2}, (■) 66.7 mA cm^{-2} and (▲) 100.0 mA cm^{-2}.

Fig. 4. Effect of herbicide concentration on the change of (a) normalized MTZ content and kinetic profiles and (b) normalized TOC and MCE with electrolysis time for the EF treatment of 100 mL of herbicide solution with 0.050 M Na_2SO_4 and 0.50 mM Fe^{2+} at pH 3.0 and 25 ºC, using a BDD/air-diffusion cell at j = 100.0 mA cm^{-2}. $[MTZ]_0$ = (◆) 0.262 mM, (▲) 0.523 mM and (▼) 1.046 mM.

Fig. 5. (a) Herbicide concentration decay and pseudo-first-order kinetic analysis, and (b) TOC abatement and MCE vs. electrolysis time for the PEF treatment of 100 mL of 0.523 mM MTZ solution with 0.050 M Na_2SO_4 and (▲) 0.50 mM Fe^{2+}or (●) 0.50 mM Fe^{3+} at pH 3.0 and 25

ºC under irradiation with a 4 W UVA lamp, using a BDD/air-diffusion cell at j = 100.0 mA cm^{-2}.

Fig. 6. Reaction sequence for MTZ degradation at pH 3.0 by EAOPs with a BDD/air-diffusion cell. The main oxidant is $^{\bullet}OH$ formed at the anode surface from water oxidation and/or in the bulk from Fenton's reaction.

Fig. 7. Evolution of (●) oxalic and (■) oxamic acids detected during the EF treatment of 100 mL of a 0.523 mM MTZ solution with 0.050 M Na_2SO_4 and 0.50 mM Fe^{2+} at pH 3.0 and 25 ºC, using a BDD/air-diffusion cell at j = 100.0 mA cm^{-2}.

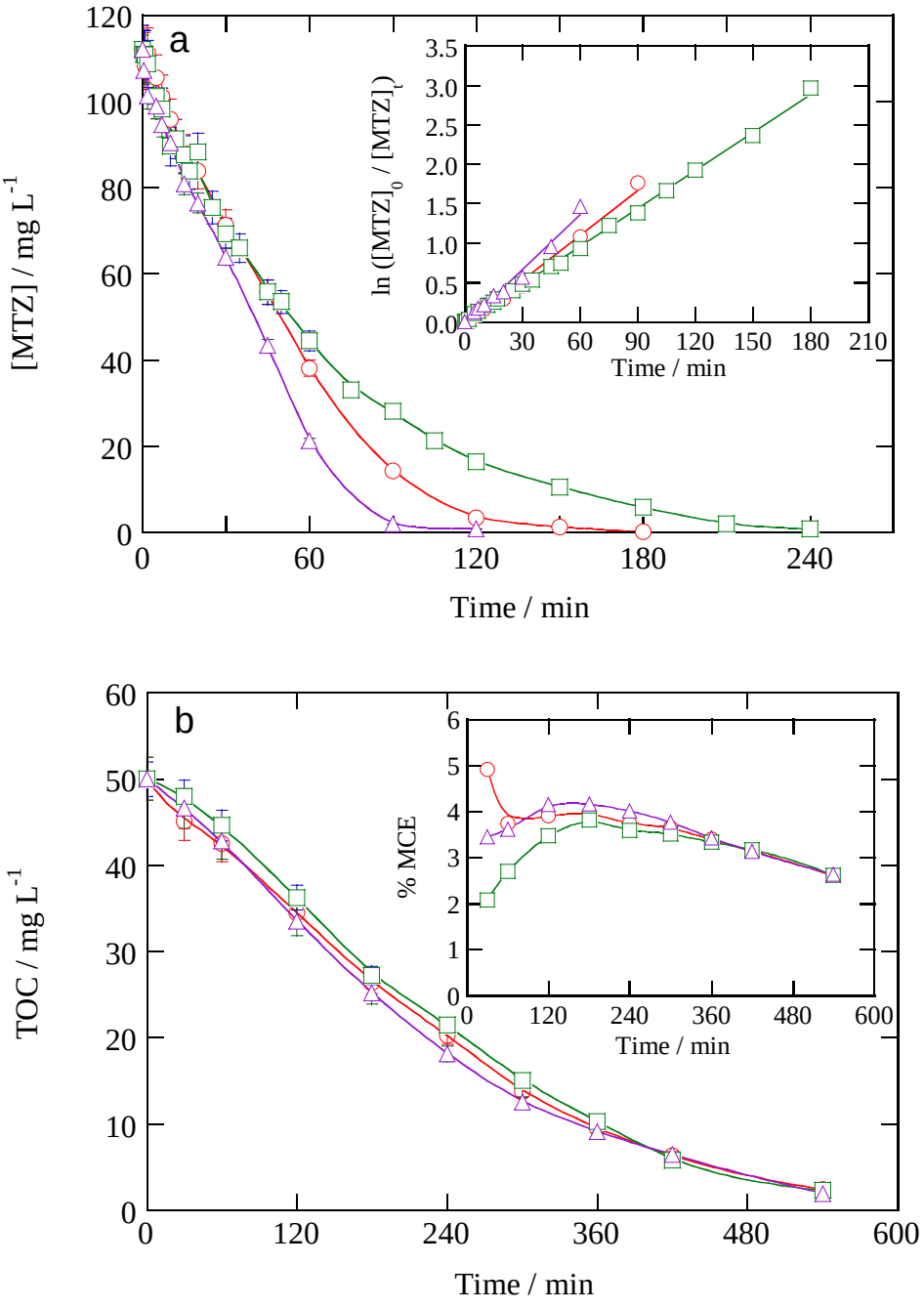
a
[MTZ] / mg L-1
Time / min
ln ([MTZ]0 / [MTZ]t)
Time / min
b
TOC / mg L-1
Time / min
% MCE
Time / min

Fig. 1

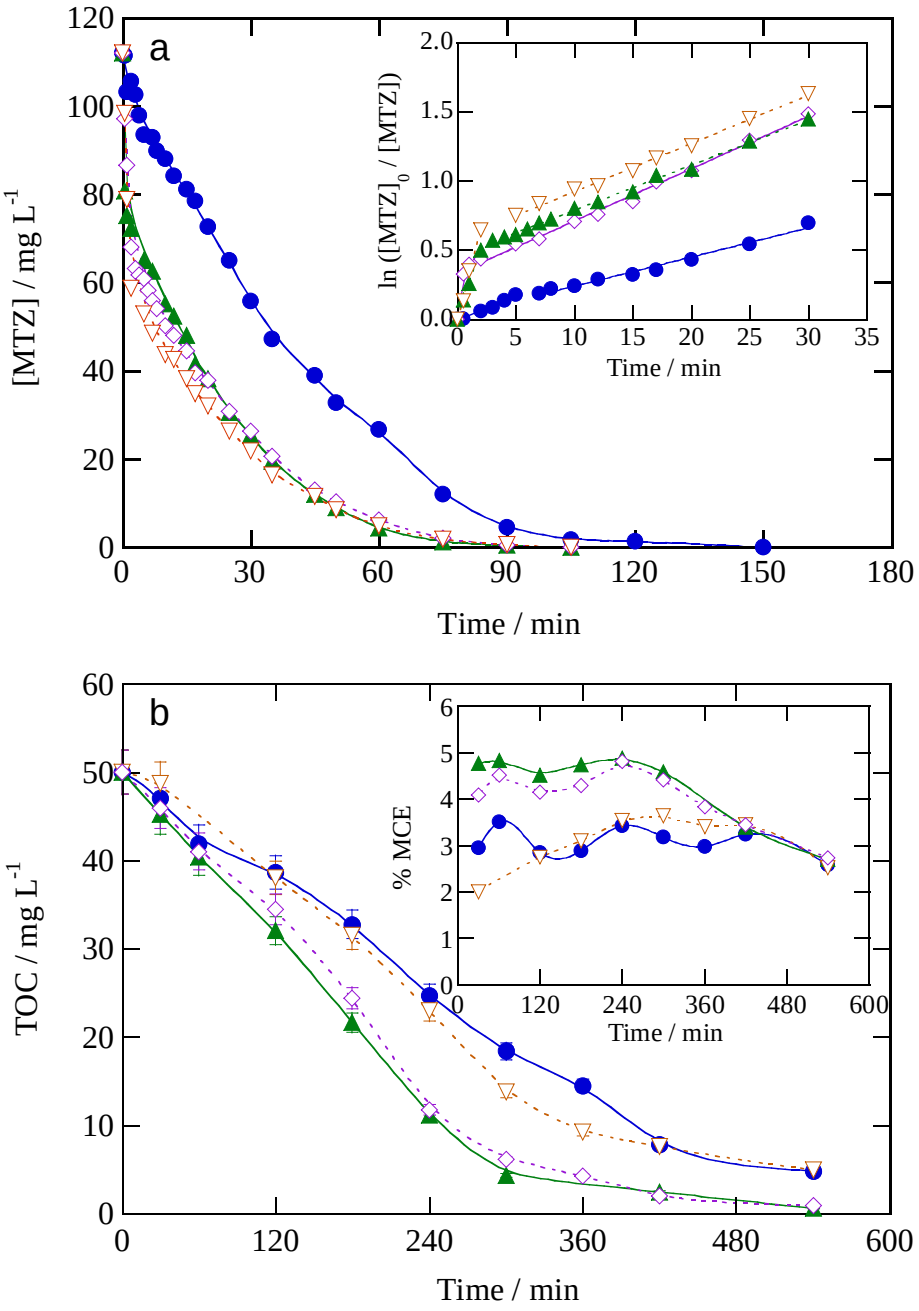
a
[MTZ] / mg L-1
Time / min
ln ([MTZ]0 / [MTZ])
Time / min
b
TOC / mg L-1
Time / min
% MCE
Time / min

Fig. 2

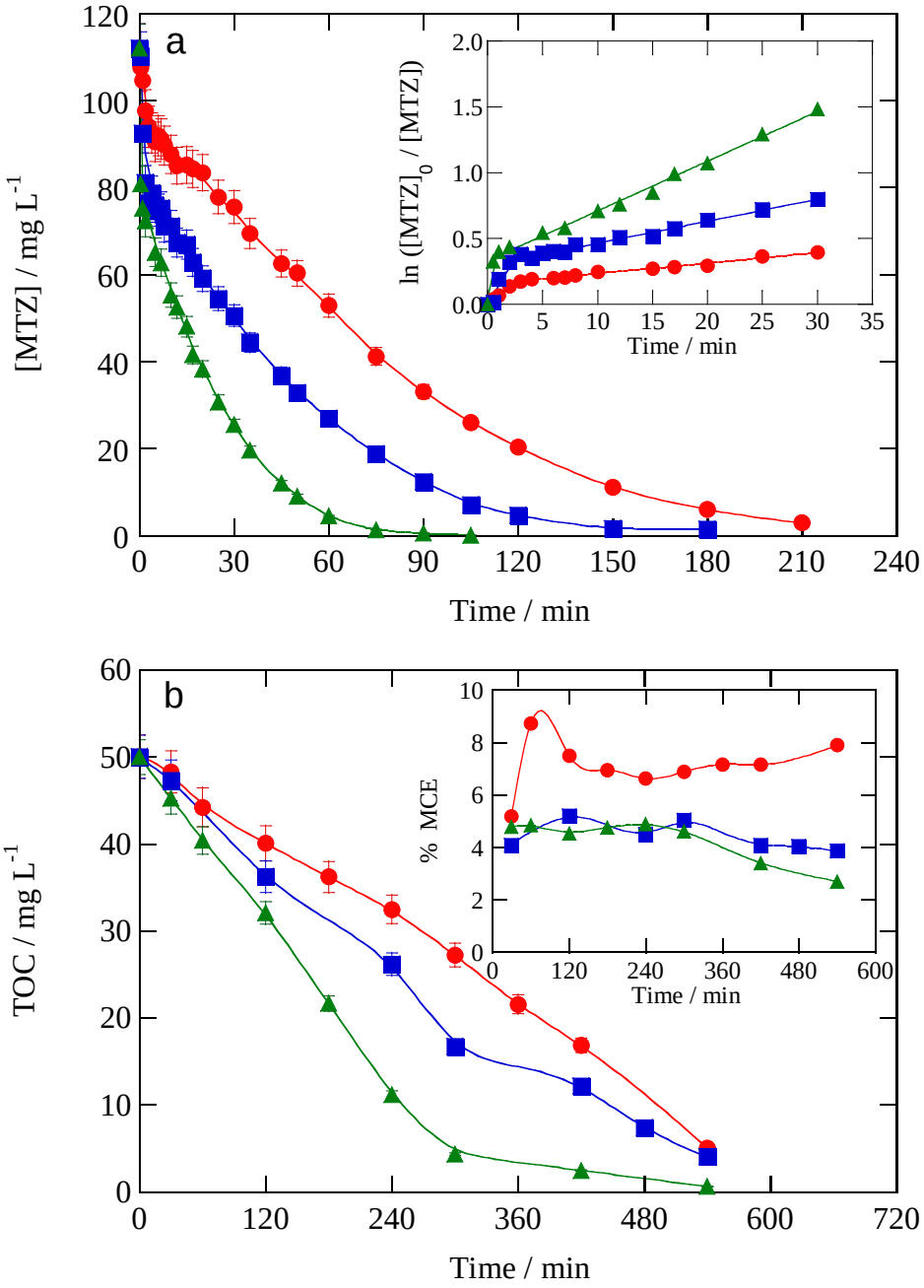
a
[MTZ] / mg L-1
Time / min
ln ([MTZ]0 / [MTZ])
Time / min
b
TOC / mg L-1
Time / min
% MCE
Time / min

Fig. 3

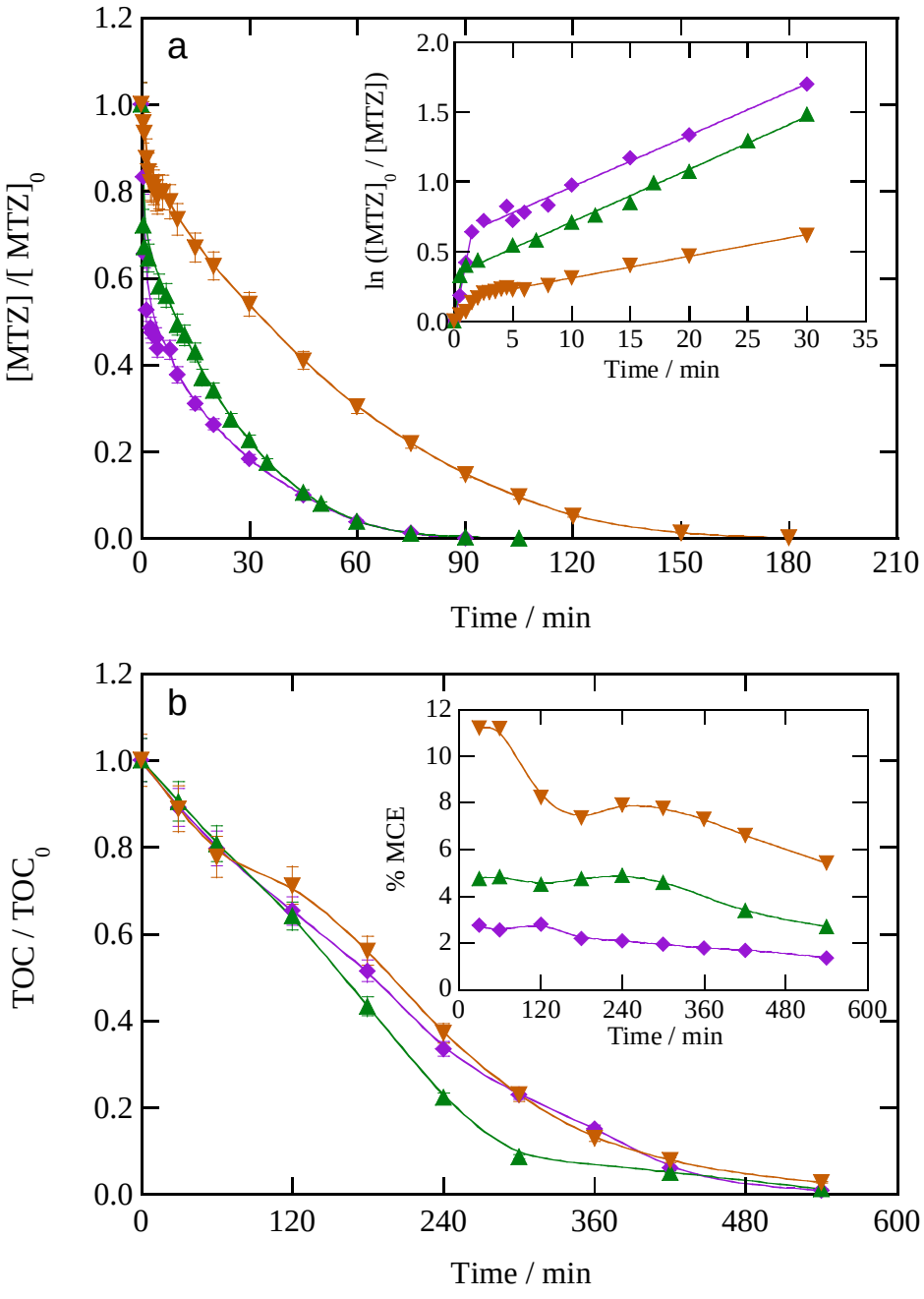
a
[MTZ] /[MTZ]0
Time / min
ln ([MTZ]0 / [MTZ])
Time / min
b
TOC / TOC0
Time / min
% MCE
Time / min

Fig. 4

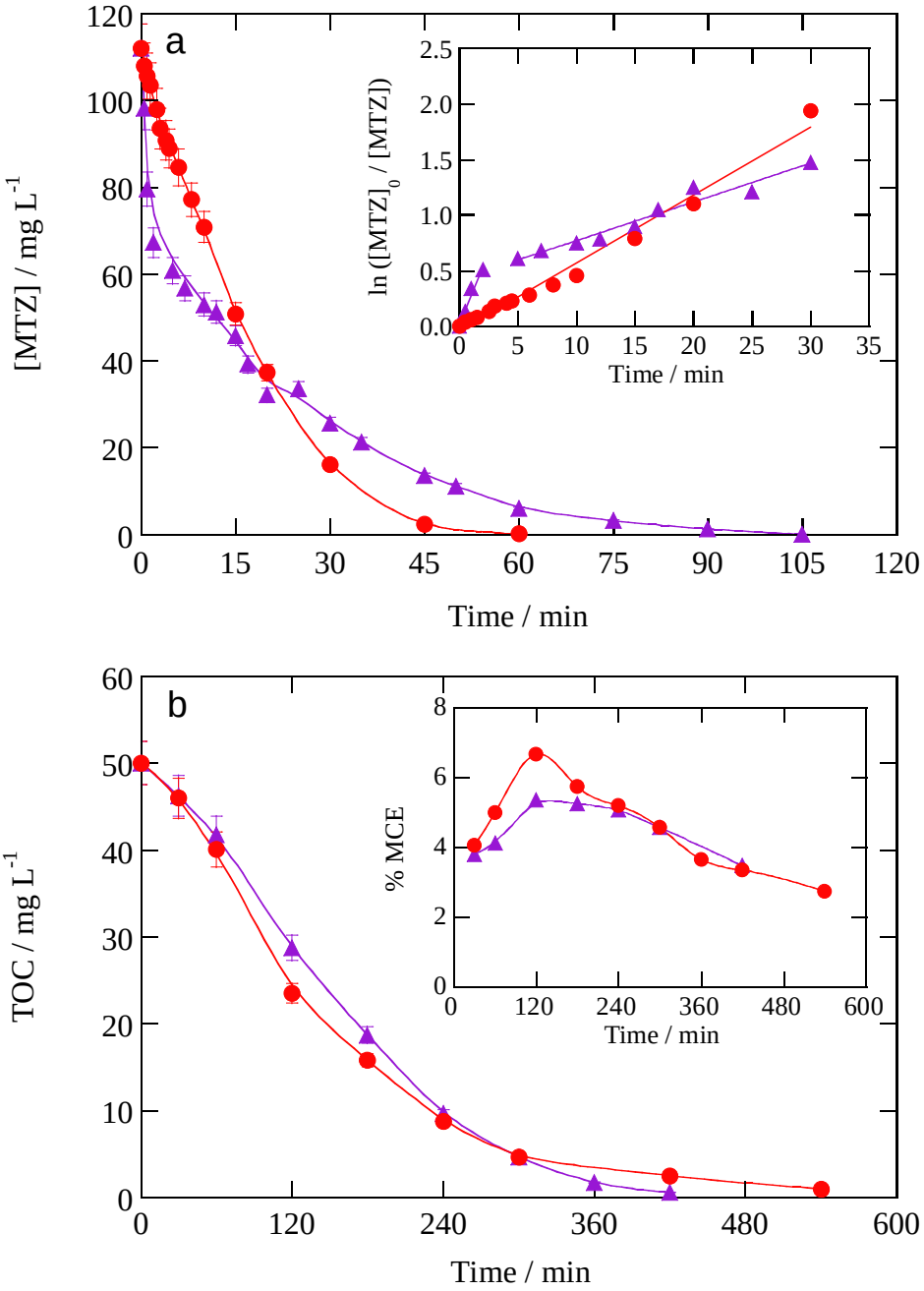
a
[MTZ] / mg L-1
Time / min
ln ([MTZ]0 / [MTZ])
Time / min
b
TOC / mg L-1
Time / min
% MCE
Time / min

Fig. 5

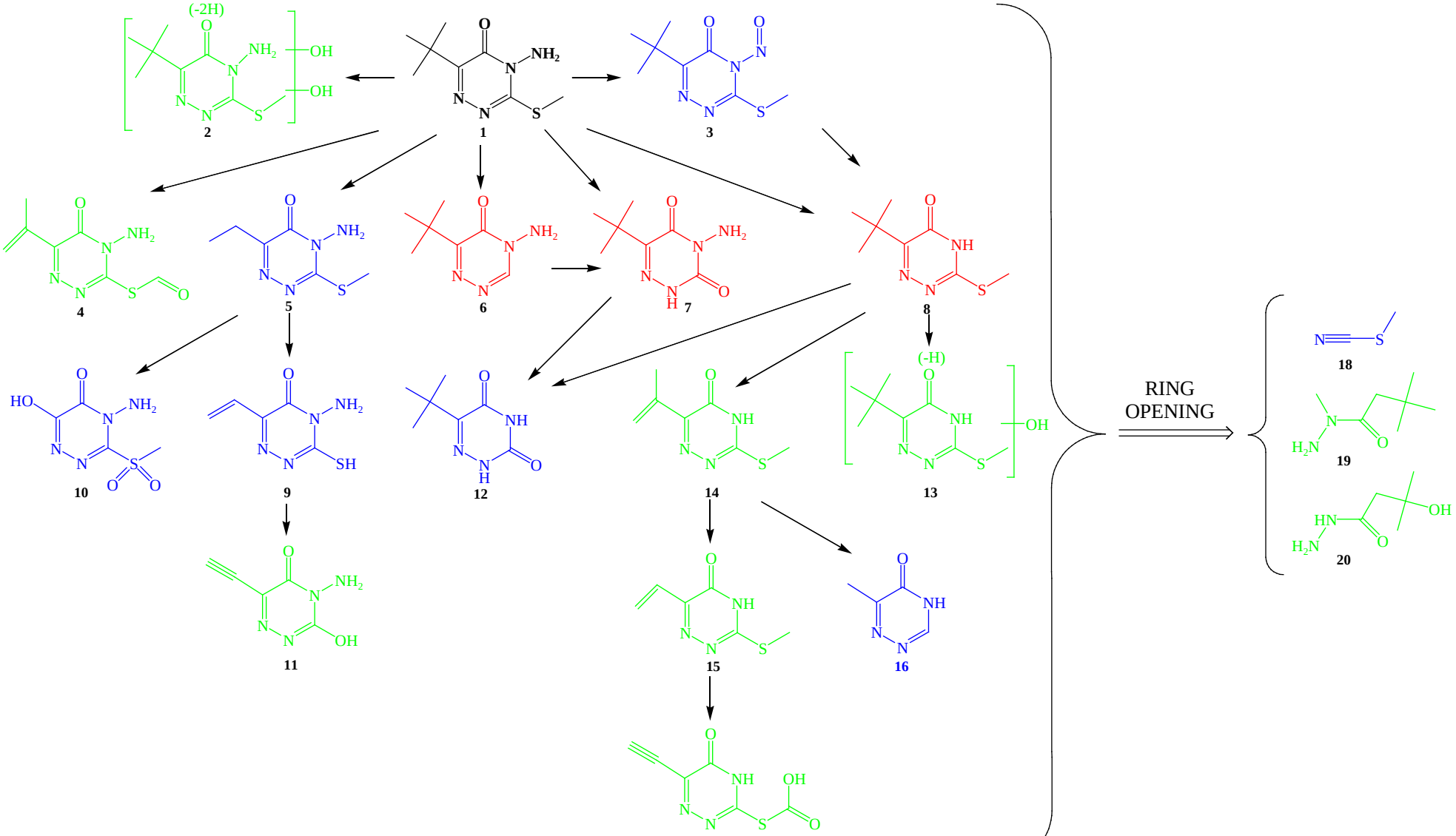
(-2H)
NH2
OH
OH
S
N
O
1
2
3
4
5
6
7
8
9
10
11
12
13
14
15
16
17
HO
SH
(-H)
NH
OH
RING
OPENING
18
19
20

Fig. 6

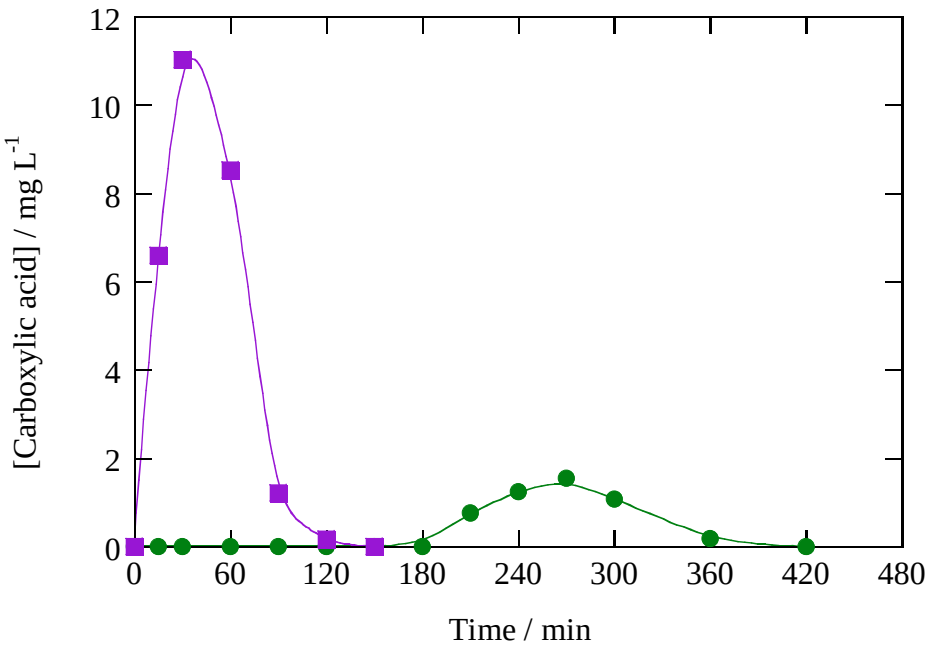
12
10
8
6
4
2
0
0
60
120
180
240
300
360
420
480
[Carboxylic acid] / mg L-1
Time / min

Fig. 7